Generalized Coherent Point Drift With Multi-Variate Gaussian Distribution and Watson Distribution

Zhe Min, Jianbang Liu, Li Liu, and Max Q.-H. Meng, *Fellow, IEEE*

***Abstract*—This letter introduces a novel rigid point set registration (PSR) approach that accurately aligns the pre-operative space and the intra-operative space together in the scenario of computer-assisted orthopedic surgery (CAOS). Motivated by considering anisotropic positional localization noise and utilizing undirected normal vectors in the point sets (PSs), the multi-variate Gaussian distribution and the Watson distribution are utilized to model positional and normal vectors' error distributions respectively. In the proposed approach, with the above probability distributions, the PSR problem is then formulated as a maximum likelihood estimation (MLE) problem and solved under the expectation maximization (EM) framework. Our contributions are three folds. First, the rigid registration problem of aligning generalized points with undirected normal vectors is formally formulated in a probabilistic manner. Second, the MLE problem is solved under the EM framework. Third, the gradients of associated objective functions with respect to desired parameters are computed and provided. Experimental results on both the human pelvis and femur models demonstrate the potential clinical values and that the proposed approach owns significantly improved performances compared with existing methods.**

***Index Terms*—Image-to-patient registration, computer-assisted orthopedic surgery (CAOS), anisotropic positional localization error, watson distribution, maximum likelihood estimation (MLE), expectation maximization (EM).**

I. Introduction

REGISTRATION finds many applications in real-world scenarios, including fields of computer vision, robotics,computer assisted surgery (CAS) and robot-assisted surgery (RAS) [2]. In computer vision, the shape reconstruction technique is utilized to reconstruct the entire 3D surface of an object [3]. More specifically, 2D images with depth information captured at different views of an interested object are first converted into 3D point sets (PSs). After that, the PSs with partial overlapping are registered together into a common global coordinate system [3]. In robotics, the registration between consecutive frames of the camera in an efficient and accurate way is essential for the robot to recover its real-time pose with respect to the surrounding environment [4]. Registration of two PSs is also a fundamental problem in CAS [5]. In CAS, the pre-operative surgical plan is tailored within the volumetric medical images (i.e., computed tomography (CT) images) while the actual surgical operation is conducted in the patient space [8]. Registration is the central operation required in a typical surgical navigation system, if it is not done well, then a guidance system may fail [6]. Thus, the pre-operative space and the intra-operative space should be accurately registered [9]–[11]. For example, a root-mean-square (RMS) error of 2 milimeters of the four controlled points is reported in the registration between the pre-operative model and the bone, in the computer-assisted reconstruction of anterior cruciate ligament (ACL) [10]. In robot-assisted orthopedic surgery (RAOS), registration is needed to map the tailored surgical plan in the pre-operative volumetric image space to the coordinate frame of surgical tool held by a robot [11]. More specifically, intra-operatively, the robot tool-tip needs to know where it is, where to go, and how to go there with respect to the real surrounding tissues. This can be achieved by identifying and locating several points(e.g. anatomical landmarks) in the pre-operative images, and the same corresponding points are touched by the robotic tool-tip. The corresponding points in the two coordinate frames are then registered together to estimate the transformation matrix between the two spaces. The disadvantage of this routine (so called fiducial-based registration) is that acquiring the corresponding landmarks can be tedious and error prone. Alternatively, PSs in can be estimated from the surface extracted from the pre-operative image, and swept over the bone surface by the robotic tool-tip. Point set registration (PSR) is used in this scenario, where the correspondences between points in two spaces are not known.

The transformation to be estimated in the registration problem can be classified into either rigid [19], [28], [39] or non-rigid [12], [13], [15]–[17]. Two iterative sub-tasks are usually involved in the rigid PSR: (1) estimates the correspondences between points in two PSs, and (2) estimates the rigid transformation matrix between two PSs using the Singular Value Decomposition (SVD) or more advanced methods [20], [21]. Registration without known point correspondences can be thought of as a "Chicken and egg" problem, which can be solved by iteratively estimating one parameter set while keeping the other parameter

Manuscript received March 2, 2021; accepted June 21, 2021. Date of publication June 28, 2021; date of current version July 22, 2021. This letter was recommended for publication by Associate Editor A. Faragasso and Editor P. Valdastri upon evaluation of the reviewers' comments. The work was supported in part by the Hong Kong Research Grants Council (RGC) General Research Fund (GRF) under Grants 14210117 and 14211420, the RGC NSFC/RGC Joint Research Scheme under Grant N_CUHK448/17, National Key R&D program of China with Grant 2019YFB1312400, and Shenzhen Science and Technology Innovation projects JCYJ20170413161503220, and in part by the Hong Kong RGC Theme-based Research Scheme (TRS) under Grant T42-409/18-R. *(Corresponding authors: Li Liu; Max Q.-H. Meng.)*

Zhe Min is with the Centre for Medical Image Computing and Wellcome/EPSRC Centre for Interventional & Surgical Sciences, University College London, London, U.K. (e-mail: z.min@ucl.ac.uk).

Jianbang Liu and Li Liu are with the Department of Electronic Engineering, The Chinese University of Hong Kong, Hong Kong (e-mail: henryliu@link.cuhk.edu.hk; leolili1212@gmail.com).

Max Q.-H. Meng is with the Department of Electronic and Electrical Engineering, Southern University of Science and Technology, Shenzhen, China, and also with the Department of Electronic Engineering, The Chinese University of Hong Kong, Hong Kong (e-mail: max.meng@ieee.org).

Digital Object Identifier 10.1109/LRA.2021.3093011

set constant. Registration problem is not a trivial task since that the acquired PSs are often disturbed with noise and outliers in real-world scenarios.

This paper introduces a novel rigid registration approach that utilizes the undirected normal vectors, which can be readily extracted from the raw PSs. Rigid PSR without known correspondence is formulated as a maximum likelihood estimation (MLE) problem, and solved under the expectation maximization (EM) framework. Multi-variate Gaussian distribution and Watson distribution are utilized to model the position localization error and the estimation error associated with the normal vectors, respectively [22]. The biggest advantage of utilizing the Watson distribution is that normal vectors do not need to point outwards consistently as that in [23].

The remainder of this paper is organized as follows. In Section II, the related PSR methods are reviewed. In Section III, we present the motivations and contributions of this paper. In Section IV, we formally define the generalized PSR problem and illustrate our approach with great details. In Section V, the results are presented. In Section VI, we conclude this paper.

II. Related Work

Registration approaches can be briefly divided into categories of Correspondence-based *and* Simultaneous Pose and Correspondence [24]. Correspondence-based registration methods first extract 3D keypoints from the raw PSs, from which the point correspondences can be constructed. For example, the Fast Point Feature Histogram (FPFH) can be used as the feature, and is further used to build the putative correspondence set [25]. Several recent approaches have been proposed by researchers belong to this category [24]. Generally speaking, our formulated registration problem and approach belong to the Simultaneous Pose and Correspondence Problem [24].

A. Iterative Closest Point (ICP) Algorithm

Iterative closest point (ICP) method is one of the most classical registration approaches [25]. Two iterative steps are involved in ICP (in the case of rigid registration): (1) estimating the point correspondences given the current transformation matrix; and (2) estimating the rigid transformation matrix given correspondences until convergence. The original ICP method has several drawbacks: (1) suffers from the local minima; (2) is susceptible to noise and outliers; (3) needs a good initialization of the rigid transformation matrix [10]. To overcome the local optimum disadvantage of the original ICP method, the Go-ICP method leverages the Branch and Bound (BnB) technique [26] On one hand, the axis-angle representation is used to represent the 3D rotation matrix and thus all rotations can be compactly represented as solid radius-π ball in 3D space. On the other hand, the optimal translation lies in the cube $[-\epsilon, \epsilon]$ where the value of ϵ could be readily large at the beginning of the algorithm. The main idea of Go-ICP, as summarized in [26], is to conduct the BnB search by taking the current objective function's value as the upper bound of following steps. Afterwards, if one better solution can be found, the original ICP algorithm is conducted to refine the solution (i.e., by reducing the objective function's value).

B. Probabilistic Registration Methods

Probabilistic registration methods can potentially improve the registration's robustness to noise and outliers with the soft assignment technique adopted to construct the point correspondences. Coherent point drift (CPD) is one of the classical probabilistic registration methods due to its robust registration performance and scalability to large-scale PSs [12]. In CPD, the source PS $\mathbf{Y}$ is assumed to be the centroids of the Gaussian Mixture Models (GMMs) while the other one $\mathbf{X}$ is considered as the data PS [12]. One recent variant of CPD is the Bayesian CPD (BCPD), where the registration problem is formulated in a Bayesian setting [27]. The advantages of BCPD over the original CPD method include the the follows. First, the convergence of BCPD is guaranteed theoretically [27]. Second, both the rigid registration and non-rigid registration steps are jointly involved in the BCPD [27]. In the expectation conditional maximization for point registration (EMCPR) method, the anisotropic positional uncertainty is considered [39]. In the maximization rigid step (i.e., where the rigid transformation matrix is updated) of the ECMPR method, the optimization of updating the rotation matrix is formulated as a semidefinite programming problem. Joint registration of multiple point clouds (JRMPC) method considers all PSs to be registered as the generalizations of an underlying mixture model [28]. The registration problem in JRMPC is formulated as a maximum likelihood estimation (MLE) problem, where the desired parameters include the rotation matrices and translation vectors that align the individual PSs with the underlying one, and the positional variance associated with the mixtures' components. The isotropic positional error assumption is shared by all above methods. Deep-learning-based methods first learn to encode PSs with high-dimensional features, then match keypoints to generate correspondence and optimize over the space of rigid transformations [29], [30], [31], [32]. However, current deep-learning based methods fail to produce acceptable inlier rates [24].

Normal vectors have been utilized to improve the PSR approaches' performances, where the von Mises-Fisher (vMF) distribution is utilized to model the estimation error associated with the normal vectors [10], [33]. For example, we have proposed several feature-based rigid registration approaches by incorporating the normal vectors into the registration problem [10], [34]. Joint registration of multiple generalized point sets was also formulated in a probabilistic manner [23], [35]–[37]. However, in the above methods, a normal vector with a specific direction is distinguished from its opposite direction, which requires the extracted normal vectors for all the points of an object's model to be pointing either outwards or inwards of the object's surface [23], [35], [36].

III. Motivations and Our Contributions

First, in many scenarios, the directions of extracted normal vectors from the raw PSs are not clear (or fixed) and the von-Mises Fisher distribution thus cannot be used. In order to overcome this disadvantage, the Watson distribution is adopted to model the undirected normal vectors' localization error. Second, most previous registration methods adopt the assumption that positional localization error is isotropic, which indicates that the error distribution is the same in three spatial directions. This paper, as far as we know, is the first one to consider both the undirected normal vector and anisotropic positional error simultaneously. Our contributions are summarized as follows:

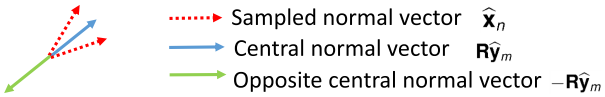

Fig. 1. $\widehat{\mathbf{x}}_n$ denotes the sampled normal vector from one probability distribution, $\mathbf{R}\widehat{\mathbf{y}}_m$ denotes the central (or model) normal vector of that distribution, and $-\mathbf{R}\widehat{\mathbf{y}}_m$ represents the opposite central normal vector. It is more appropriate to utilize the Watson distribution to describe the error distribution between the un-directed normal vectors.

1) The PSR problem of aligning generalized points with undirected normal vectors is formally formulated as a maximum likelihood estimation (MLE) problem, with the multi-variate Gaussian distribution and Watson distribution.
2) The MLE problem is solved with expectation maximization (EM) technique, where the equations of the updated involved parameters are derived and presented.
3) To facilitate the computing process, the gradients of associated objective function with respect to the desired parameters are computed and provided. The parameters include these that represent the incremental transformation matrix, the positional covariance matrix, and the concentration parameter associated with the normal vectors' error.

IV. Approach

In our proposed approach, the generalized/oriented points in two spaces $\mathbf{d}_n^x = [\mathbf{x}_n^\mathsf{T}, \widehat{\mathbf{x}}_n^\mathsf{T}]^\mathsf{T} \in \mathbb{R}^6$ and $\mathbf{d}_m^y = [\mathbf{y}_m^\mathsf{T}, \widehat{\mathbf{y}}_m^\mathsf{T}]^\mathsf{T} \in \mathbb{R}^6$ are utilized, where $\mathbf{x}_n \in \mathbb{R}^3$ and $\widehat{\mathbf{x}}_n \in \mathbb{R}^3$ denote the positional and normal vectors respectively.Let us also denote the two generalized point sets (PSs) as $\mathbf{D}_x = [\mathbf{d}_1^x, \ldots, \mathbf{d}_N^x] \in \mathbb{R}^{6\times N}$ and $\mathbf{D}_y = [\mathbf{d}_1^y, \ldots, \mathbf{d}_M^y] \in \mathbb{R}^{6\times M}$. By assuming that $\mathbf{D}_x$ and $\mathbf{D}_y$ are independent, the probability density function (PDF) of a generalized data point $\mathbf{d}_n^x$ generated by a generalized model point $\mathbf{d}_m^y$ is given as follows

$$p(\mathbf{d}_n^x|z_n = m, \mathbf{\Theta}) = \underbrace{\frac{1}{(2\pi)^{\frac{3}{2}}|\mathbf{\Sigma}|^{\frac{1}{2}}} e^{-\frac{1}{2}\mathbf{z}_{mn}^\mathsf{T}\mathbf{\Sigma}^{-1}\mathbf{z}_{mn}}}_{\text{Multi-variate˜Gaussian}} \underbrace{W(\frac{1}{2}, \frac{3}{2}, \kappa)^{-1} e^{\kappa\left((\mathbf{R}\widehat{\mathbf{y}}_m)^\mathsf{T}\widehat{\mathbf{x}}_n\right)^2}}_{\text{Watson˜ Distribution}}, \tag{1}$$

where $z_n = m$ indicates that the n-th generalized data point $\mathbf{d}_n^x$ corresponds to the m-th generalized model point $\mathbf{d}_m^y$, $\mathbf{\Sigma} \in \mathbb{S}^3$ is the positional covariance matrix, $\mathbf{z}_{mn} = (\mathbf{x}_n - (\mathbf{R}\mathbf{y}_m + \mathbf{t})) \in \mathbb{R}^3$ is the distance vector between the n-th data point $\mathbf{x}_n$ and the m-th rigidly transformed model point $\mathbf{R}\mathbf{y}_m + \mathbf{t}$, $W(\frac{1}{2}, \frac{3}{2}, \kappa)^{-1}$ is the normalizing constant associated with the Watson distribution [22], [38], $\kappa \in \mathbb{R}$ is the concentration parameter associated with the Watson distribution [22], [38], $\mathbf{z}_{mn}^\mathsf{T}\mathbf{\Sigma}^{-1}\mathbf{z}_{mn}$ is the square of the Mahalanobis distance between $\mathbf{x}_n$ and $\mathbf{R}\mathbf{y}_m + \mathbf{t}$.

Assume that the angle between $\mathbf{R}\widehat{\mathbf{y}}_m$ and $\widehat{\mathbf{x}}_n$ is $\alpha \in \mathbb{R}$. As shown in Fig. 1, (1) $(\mathbf{R}\widehat{\mathbf{y}}_m)^\mathsf{T}\widehat{\mathbf{x}}_n = \cos(\alpha)$ where $\mathbf{R}\widehat{\mathbf{y}}_m$ and $\widehat{\mathbf{x}}_n$ are used;(2) $-(\mathbf{R}\widehat{\mathbf{y}}_m)^\mathsf{T}\widehat{\mathbf{x}}_n = -\cos(\alpha)$ where $-\mathbf{R}\widehat{\mathbf{y}}_m$ and $\widehat{\mathbf{x}}_n$ are used (i.e., $-(\mathbf{R}\widehat{\mathbf{y}}_m)$ is the central(or model) normal vector of the probability distribution). By taking square of $\cos(\alpha)$ or $-\cos(\alpha)$, it makes no difference in the PDF value.

With the above analysis, the hybrid mixture model (HMM) of one generalized data point $\mathbf{d}_n^x$ is, given $\mathbf{D}_y$ and $\mathbf{\Theta}$,

$$p(\mathbf{d}_n^x|\mathbf{D}_y, \mathbf{\Theta}) = (1-w)\sum_{m=1}^{M} p(\mathbf{d}_n^x|z_n = m, \mathbf{\Theta}) + w\frac{1}{N}, \tag{2}$$

where $w \in \mathbb{R}$ denotes the weight of outliers, whose distribution is uniform as $p(\mathbf{d}_n^x|z_n = M+1) = \frac{1}{N}$ (where $z_n = M+1$ indicates that $\mathbf{d}_n^x$ is an outlier).

By formulating the negative log-likelihood similar to those in [10], [34], the overall objective function $Q(\mathbf{\Theta})$ is as follows,

$$\begin{aligned} Q(\mathbf{\Theta}) = &\sum_{n,m=1}^{N,M} p_{mn}\frac{1}{2}\mathbf{z}_{mn}^\mathsf{T}\mathbf{\Sigma}^{-1}\mathbf{z}_{mn} + \frac{1}{2}N_\mathbf{P}\log|\mathbf{\Sigma}| \\ &- \kappa\sum_{n,m=1}^{N,M} p_{mn}\left((\mathbf{R}\widehat{\mathbf{y}}_m)^\mathsf{T}\widehat{\mathbf{x}}_n\right)^2 - N_\mathbf{P}\log W(\frac{1}{2}, \frac{3}{2}, \kappa)^{-1}, \end{aligned} \tag{3}$$

where $N_\mathbf{P} = \sum_{n=1}^{N}\sum_{m=1}^{M} p_{mn} \in \mathbb{R}$ is the sum of posterior probabilities, $|\mathbf{\Sigma}|$ denotes the determinant of $\mathbf{\Sigma}$. The derivation of $Q(\mathbf{\Theta})$ in (3) is presented in Section VII-B. $Q(\mathbf{\Theta})$ is minimized with respect to the parameter set $\mathbf{\Theta} = (\mathbf{R}, \mathbf{t}, \mathbf{\Sigma}, \kappa, \{p_{mn}\})$. The expectation maximization (EM) technique is used to solve the above maximum likelihood estimation (MLE) problem with unknown correspondences.

A. Expectation Step

The posterior p_{mn} is updated as follows with the Bayes' rule,

$$p_{mn} = \frac{P(m)p(\mathbf{d}_n^x|z_n = m, \mathbf{\Theta})}{p(\mathbf{d}_n^x|\mathbf{D}_y, \mathbf{\Theta})}, \tag{4}$$

where $p(\mathbf{d}_n^x|z_n = m, \mathbf{\Theta})$ is presented in (1), $P(m)$ is the prior probability, and $p(\mathbf{d}_n^x|\mathbf{D}_y, \mathbf{\Theta})$ is given in (2). Then the detailed expression of p_{mn} is

$$p_{mn} = \frac{g e^{-\frac{1}{2}\mathbf{z}_{mn}^\mathsf{T}\mathbf{\Sigma}^{-1}\mathbf{z}_{mn}} e^{\kappa\left((\mathbf{R}\widehat{\mathbf{y}}_m)^\mathsf{T}\widehat{\mathbf{x}}_n\right)^2}}{\sum_{m=1}^{M} g e^{-\frac{1}{2}\mathbf{z}_{mn}^\mathsf{T}\mathbf{\Sigma}^{-1}\mathbf{z}_{mn}} e^{\kappa((\mathbf{R}\widehat{\mathbf{y}}_m)^\mathsf{T}\widehat{\mathbf{x}}_n)^2} + \frac{wM}{(1-w)N}}, \tag{5}$$

where $g = \frac{1}{(2\pi)^{\frac{3}{2}}|\mathbf{\Sigma}|^{\frac{1}{2}}} W(\frac{1}{2}, \frac{3}{2}, \kappa)^{-1}$, and the derivation is presented in Section. VII-A.

B. Maximization Rigid Step

The terms in $Q(\mathbf{\Theta})$ in (3) that are related with $(\mathbf{R}, \mathbf{t})$ is as follows

$$\begin{aligned} Q(\mathbf{R}, \mathbf{t}) = &\sum_{n,m=1}^{N,M} p_{mn}\frac{1}{2}\mathbf{z}_{mn}^\mathsf{T}\mathbf{\Sigma}^{-1}\mathbf{z}_{mn} \\ &- \kappa\sum_{n,m=1}^{N,M} p_{mn}\left((\mathbf{R}\widehat{\mathbf{y}}_m)^\mathsf{T}\widehat{\mathbf{x}}_n\right)^2 - \sum_{n,m=1}^{N,M} p_{mn}\frac{1}{2}\mathbf{x}_n^\mathsf{T}\mathbf{\Sigma}^{-1}\mathbf{x}_n. \end{aligned} \tag{6}$$

Instead of estimating the $\mathbf{R}$ and $\mathbf{t}$, we update the incremental rotation matrix $d\mathbf{R} \in SO(3)$ and the incremental translation

vector $d\mathbf{t} \in \mathbb{R}^3$ between two iterated M steps, where the objective function of $d\mathbf{R}$ and $d\mathbf{t}$ becomes

$$Q(d\mathbf{R}, d\mathbf{t}) = \sum_{n,m=1}^{N,M} \underbrace{p_{mn}\left(\frac{1}{2}\mathbf{z}_{mn}^{\text{new}\,\mathsf{T}}\boldsymbol{\Sigma}^{-1}\mathbf{z}_{mn}^{\text{new}} - \frac{1}{2}\mathbf{x}_n^{\mathsf{T}}\boldsymbol{\Sigma}^{-1}\mathbf{x}_n\right)}_{C_{P,mn}\in\mathbb{R}} - \kappa \sum_{n,m=1}^{N,M} \underbrace{p_{mn}\left((d\mathbf{R}\widehat{\mathbf{y}}_m)^{\mathsf{T}}\widehat{\mathbf{x}}_n\right)^2}_{C_{O,mn}\in\mathbb{R}}, \tag{7}$$

where $\mathbf{z}_{mn}^{\text{new}} = (\mathbf{x}_n - d\mathbf{R}(\mathbf{R}\mathbf{y}_m + \mathbf{t}) - d\mathbf{t}) \in \mathbb{R}^3$. Two nonlinear constraints have to be satisfied when $Q(d\mathbf{R}, d\mathbf{t})$ is minimized: $d\mathbf{R}d\mathbf{R}^{\mathsf{T}} = \mathbf{I}_{3\times3}, det(d\mathbf{R}) = +1$.

The Matrix Form of $\sum_{n=1}^{N}\sum_{m=1}^{M} C_{O,mn}$ We first construct the matrix $\mathbf{A} \in \mathbb{R}^{M\times N}$ as follows,

$$\mathbf{A} = \begin{bmatrix} (d\mathbf{R}\mathbf{R}\widehat{\mathbf{y}}_1)^{\mathsf{T}}\widehat{\mathbf{x}}_1 & \dots & (d\mathbf{R}\mathbf{R}\widehat{\mathbf{y}}_1)^{\mathsf{T}}\widehat{\mathbf{x}}_N \\ . & \dots & . \\ . & \dots & . \\ . & \dots & . \\ (d\mathbf{R}\mathbf{R}\widehat{\mathbf{y}}_M)^{\mathsf{T}}\widehat{\mathbf{x}}_1 & \dots & (d\mathbf{R}\mathbf{R}\widehat{\mathbf{y}}_M)^{\mathsf{T}}\widehat{\mathbf{x}}_N \end{bmatrix} \in \mathbb{R}^{M\times N}, \tag{8}$$

or $\mathbf{A} = (d\mathbf{R}\mathbf{R}\widehat{\mathbf{Y}})^{\mathsf{T}}\widehat{\mathbf{X}}$. With $\mathbf{A}$, we can get $\sum_{n=1}^{N}\sum_{m=1}^{M} C_{O,mn}$ as follows

$$\sum_{n,m=1}^{N,M} C_{O,mn} = -\kappa\mathbf{e}^{\mathsf{T}}\mathbf{A}\circ\mathbf{A}\circ\mathbf{P}. \tag{9}$$

We use the Rodrigues formula to represent the incremental rotation matrix $d\mathbf{R}$ between iterative steps,

$$\mathbf{R}(\boldsymbol{\theta}) = \mathbf{I} + \frac{\sin(\vartheta)}{\vartheta}[\boldsymbol{\theta}]_\times + \frac{1-\cos(\vartheta)}{\vartheta^2}[\boldsymbol{\theta}]_\times^2, \tag{10}$$

which is actually a function that maps a vector $\boldsymbol{\theta} \in \mathbb{R}^3$ into a 3D rotation matrix $\mathbb{R}$, $\vartheta = ||\boldsymbol{\theta}||$ denotes the norm of the vector $\boldsymbol{\theta}$, and the skew symmetric matrix $[\boldsymbol{\theta}]_\times$ is defined as follows, $[\boldsymbol{\theta}]_\times = [0, -\theta_3, \theta_2; \theta_3, 0, -\theta_1; -\theta_2, \theta_1, 0]$. In other words, the incremental rotation matrix $d\mathbf{R}$ in the $SO(3)$ is now represented by a random vector $d\boldsymbol{\theta} \in \mathbb{R}^3$. Let us also formulate a new variable $\phi = [d\boldsymbol{\theta}^{\mathsf{T}}, d\mathbf{t}^{\mathsf{T}}]^{\mathsf{T}} \in \mathbb{R}^6$. Thus, we can convert $Q(d\mathbf{R}, d\mathbf{t})$ in (7) into an unconstrained optimization problem with the objective function $Q(\phi)$ being

$$Q(\phi) = \sum_{n,m=1}^{N,M} \underbrace{p_{mn}\left(\frac{1}{2}\mathbf{z}_{mn}^{\text{new},2\,\mathsf{T}}\boldsymbol{\Sigma}^{-1}\mathbf{z}_{mn}^{\text{new},2} - \frac{1}{2}\mathbf{x}_n^{\mathsf{T}}\boldsymbol{\Sigma}^{-1}\mathbf{x}_n\right)}_{C_{P,mn}\in\mathbb{R}} - \kappa \sum_{n,m=1}^{N,M} \underbrace{p_{mn}\left((\mathbf{R}(\phi(1:3))\widehat{\mathbf{y}}_m)^{\mathsf{T}}\widehat{\mathbf{x}}_n\right)^2}_{C_{N,mn}\in\mathbb{R}}, \tag{11}$$

where $\mathbf{z}_{mn}^{\text{new},2} == (\mathbf{x}_n - \mathbf{R}(d\theta)(\mathbf{R}\mathbf{y}_m + \mathbf{t}) - d\mathbf{t}) \in \mathbb{R}^3$. **The Gradients of** $C_{O,mn}$ **with respect to the** $\mathbf{dR}$ The derivative of $C_{O,mn}$ with respect to $d\mathbf{R}$ is $\frac{\partial C_{O,mn}}{\partial d\mathbf{R}} = -2\kappa p_{mn}\widehat{\mathbf{x}}_n\widehat{\mathbf{x}}_n^{\mathsf{T}}d\mathbf{R}\mathbf{R}\widehat{\mathbf{y}}_m\widehat{\mathbf{y}}_m^{\mathsf{T}}\mathbf{R}^{\mathsf{T}}$. After estimating the incremental rotation $d\mathbf{R}$ and $d\mathbf{t}$, the 3D rotation and translation in the current step can be updated as $\mathbf{R}^q = d\mathbf{R}\mathbf{R}^{q-1}, \mathbf{t}^q = d\mathbf{R}\mathbf{t}^{q-1} + d\mathbf{t}$ respectively.

C. Maximization Covariance Step

The objective function that is related with $\boldsymbol{\Sigma}$ is given as follows $Q(\boldsymbol{\Sigma}) = \sum_{n=1}^{N}\sum_{m=1}^{M} p_{mn}\frac{1}{2}\mathbf{z}_{mn}^{\mathsf{T}}\boldsymbol{\Sigma}^{-1}\mathbf{z}_{mn} + \frac{1}{2}N_{\mathbf{P}}\log|\boldsymbol{\Sigma}| - \sum_{n=1}^{N}\sum_{m=1}^{M} p_{mn}\frac{1}{2}\mathbf{x}_n^{\mathsf{T}}\boldsymbol{\Sigma}^{-1}\mathbf{x}_n$. The matrix form of the updated positional covariance matrix $\boldsymbol{\Sigma}$ is

$$\begin{aligned}&\left(\mathbf{X}\text{diag}\left(\mathbf{P}^{\mathsf{T}}\mathbf{e}\right)\mathbf{X}^{\mathsf{T}} - \mathbf{X}\mathbf{P}^{\mathsf{T}}\mathbf{e}(\mathbf{t}^q)^{\mathsf{T}} - \mathbf{t}^q\mathbf{e}^{\mathsf{T}}\mathbf{P}\mathbf{X}^{\mathsf{T}} + \mathbf{R}^q\mathbf{Y}\mathbf{P}\mathbf{e}(\mathbf{t}^q)^{\mathsf{T}}\right.\\ &+ (\mathbf{t}^q)\mathbf{e}^{\mathsf{T}}\mathbf{P}^{\mathsf{T}}\mathbf{Y}^{\mathsf{T}}(\mathbf{R}^q)^{\mathsf{T}} - \mathbf{R}^q\mathbf{Y}\mathbf{P}\mathbf{X}^{\mathsf{T}} - \mathbf{X}\mathbf{P}^{\mathsf{T}}\mathbf{Y}^{\mathsf{T}}(\mathbf{R}^q)^{\mathsf{T}}\\ &\left.+ \mathbf{t}^q(\mathbf{t}^q)^{\mathsf{T}}N_{\mathbf{P}}^q + \mathbf{R}^q\mathbf{Y}\text{diag}(\mathbf{P}\mathbf{e})\mathbf{Y}\mathbf{P}^{\mathsf{T}}(\mathbf{R}^q)^{\mathsf{T}}\right)/N_{\mathbf{P}}^q,\end{aligned} \tag{12}$$

where $q \in N_+$ represents the index of the iterative EM steps.

D. Maximization Kappa Step

The objective function $Q(\kappa)$ that is related with κ is given as follows, $Q(\kappa) = -\kappa\sum_{n=1}^{N}\sum_{m=1}^{M} p_{mn}((\mathbf{R}\widehat{\mathbf{y}}_m)^{\mathsf{T}}\widehat{\mathbf{x}}_n)^2 - N_{\mathbf{P}}\log W(\frac{1}{2}, \frac{3}{2}, \kappa)^{-1}$, whose the Gradient is given as follows,

$$\frac{\partial Q(\kappa)}{\partial\kappa} = -\sum_{n=1}^{N}\sum_{m=1}^{M} p_{mn}\left((\mathbf{R}\widehat{\mathbf{y}}_m)^{\mathsf{T}}\widehat{\mathbf{x}}_n\right)^2 + N_{\mathbf{P}}\frac{W'(\frac{1}{2}, \frac{3}{2}, \kappa)}{W(\frac{1}{2}, \frac{3}{2}, \kappa)}, \tag{13}$$

where $W'(\frac{1}{2}, \frac{3}{2}, \kappa)$ denotes the derivative of $W(\frac{1}{2}, \frac{3}{2}, \kappa)$ with respect to κ. The value of the updated κ is acquired by solving $\frac{\partial Q(\kappa)}{\partial\kappa} = 0$.

The updating of κ Let us first construct $r_1 = \sum_{n=1}^{N}\sum_{m=1}^{M} p_{mn}((\mathbf{R}\widehat{\mathbf{y}}_m)^{\mathsf{T}}\widehat{\mathbf{x}}_n)^2/N_{\mathbf{P}}, r_2 = \frac{\sum_{n=1}^{N}\sum_{m=1}^{M} p_{mn}\mathbf{x}_n'\mathbf{R}\mathbf{y}_m'}{\sum_{n=1}^{N}\sum_{m=1}^{M} p_{mn}||\mathbf{x}_n'||||\mathbf{R}\mathbf{y}_m'||}$, where $\mathbf{x}_n' \in \mathbb{R}^3$ and $\mathbf{y}_m' \in \mathbb{R}^3$ are the demeaned vectors. Then with $r = \frac{1}{2}r_1 + \frac{1}{2}r_2$, the updated concentration parameter is $\kappa = \frac{\frac{3}{2}r - \frac{1}{2}}{r(1-r)} + \frac{r}{3(1-r)}$. The matrix forms of r_1 and r_2 are in Section. VII-C.

E. Implementation Details

The initial rotation matrix $\mathbf{R}^0$ and translation vector $\mathbf{t}^0$, at the beginning of the algorithm, are the three-by-three identity matrix $\mathbf{I}_{3\times3}$ and three-dimensional zero vector $\mathbf{0}_{3\times1}$. The weight w is 0.5. The initial positional covariance matrix $\boldsymbol{\Sigma}^0$ and κ^0, at the beginning of the algorithm, are set to be $\boldsymbol{\Sigma}^0 = \text{diag}([100100, 100])$ and $\kappa^0 = 20$.

V. Results

In the scenario of computer-assisted surgery (CAS), $\mathbf{Y}$ denote the pre-operative model while $\mathbf{X}$ represent the intra-operative points. In the following experiments, $M = 1568$ points exist in the model point set (PS) $\mathbf{Y}$ while $N_{\text{inliers}} = 100$ inlier points exist in the data PS $\mathbf{X}$. The inlier points $\mathbf{X}$ can be acquired with optically tracked surgical pointer. The model PS $\mathbf{Y}$ is extracted from the surface segmented from the pre-operative CT images. $\mathbf{X}$ and $\mathbf{Y}$ are from one patient. To test the robustness of our proposed approach with respect to noise and outliers, randomly generated positional and normal error vectors are injected to $\mathbf{X}$. Five cases are tested where $\{10\%, 30\%, 50\%, 70\%, 90\%\}$ outliers are injected respectively. More specifically, in the case of 10% outliers, there are $N = N_{\text{inliers}}(1 + 10\%) = 110$ points in $\mathbf{X}$, which is a common way for producing outliers in the research of point set registration. Two types of positional error are tested for each case of certain percentage of outliers. In the case of

TABLE I
ROTATIONAL ERROR VALUES IN DEGREE AND TRANSLATION ERROR VALUES IN MM ON THE HUMAN PELVIC MODEL. ISOTROPIC (DENOTED AS ISO) AND ANISOTROPIC (DENOTED AS ANISO) POSITIONAL NOISE VECTORS ARE INJECTED INTO $\mathbf{X}$, RESPECTIVELY

	Outliers	10%	30%	50%	70%	90%	10%	30%	50%	70%	90%
Iso		Rotational Error (in degree)					Translational Error (in mm)				
	ICP[25]	0.342	1.102	1.138	1.211	0.879	0.310	0.620	0.818	1.237	1.026
	CPD[12]	2.533	2.778	2.635	3.038	3.112	2.197	2.257	2.411	2.474	2.510
	ECMPR[39]	1.863	1.843	1.942	1.549	1.481	1.483	1.375	1.392	1.172	1.153
	Go-ICP[26]	0.342	0.729	1.036	1.039	1.155	0.331	0.351	0.721	0.868	1.106
	JRMPC[28]	0.431	0.472	0.357	0.443	0.425	0.400	0.441	0.388	0.270	0.402
	DGR[31]	0.323	0.812	1.076	1.354	1.512	0.296	0.591	0.778	1.063	1.241
	HMM(Iso) [40]	0.3886	0.3895	0.4197	0.4012	0.3931	0.3527	0.3515	0.3576	0.3485	0.3552
	Ours	**0.1490**	**0.1454**	**0.1399**	**0.1405**	**0.1323**	**0.1319**	**0.1291**	**0.1274**	**0.1274**	**0.1224**
Aniso	Outliers	10%	30%	50%	70%	90%	10%	30%	50%	70%	90%
		Rotational Error (in degree)					Translational Error (in mm)				
	ICP[25]	0.504	0.615	0.9892	1.560	1.414	0.254	0.561	0.520	1.002	1.123
	CPD[12]	2.059	2.256	2.191	2.522	2.715	2.035	2.188	2.276	2.219	2.342
	ECMPR[39]	1.562	1.528	1.245	1.297	1.049	1.336	1.251	1.120	1.034	0.924
	Go-ICP[26]	0.504	0.606	0.990	1.484	1.767	0.342	0.531	0.547	0.959	1.251
	JRMPC[28]	0.336	0.366	0.445	0.415	0.332	0.345	0.390	0.576	0.415	0.433
	DGR[31]	0.298	0.516	0.713	1.049	1.120	0.225	0.307	0.528	0.871	1.034
	HMM(Iso) [40]	0.2439	0.2635	0.2479	0.2601	0.2252	0.3038	0.2952	0.3051	0.3171	0.2984
	Ours	**0.0832**	**0.0871**	**0.0867**	**0.0869**	**0.0857**	**0.0920**	**0.0962**	**0.0941**	**0.0935**	**0.0914**

TABLE II
THE TARGET REGISTRATION ERROR (TRE) VALUES ON BOTH THE HUMAN PELVIC AND FEMUR MODELS. ISOTROPIC (DENOTED AS ISO) AND ANISOTROPIC (DENOTED AS ANISO) POSITIONAL NOISE VECTORS ARE INJECTED INTO $\mathbf{X}$ WITH DIFFERENT PERCENTAGES OF OUTLIERS

	Outliers	10%	30%	50%	70%	90%	10%	30%	50%	70%	90%
Pelvis	TRE statistics	Isotropic Positional Noise					Anisotropic Positional Noise				
	Maximum Value	**0.7559**	0.5243	0.5071	0.5222	0.5052	0.2623	0.2751	0.2637	0.2595	0.2595
	Mean Value	0.3082	0.1697	0.1653	0.1643	0.1577	0.1089	0.1191	0.1174	0.1168	0.1146
	Minimum Value	0.0121	0.0328	0.0343	0.0366	0.0298	0.0273	0.0268	0.0294	0.0290	0.0271
Femur	Outliers	10%	30%	50%	70%	90%	10%	30%	50%	70%	90%
	TRE statistics	Isotropic Positional Noise					Anisotropic Positional Noise				
	Maximum Value	**0.8275**	0.7442	0.8168	0.7933	0.7123	0.7493	0.6766	0.6685	0.6314	0.6537
	Mean Value	0.3549	0.3368	0.3677	0.3582	0.3238	0.3462	0.3140	0.3051	0.2927	0.3082
	Minimum Value	0.0409	0.0540	0.0624	0.0563	0.0589	0.0696	0.0612	0.0489	0.0522	0.0507

isotropic positional noise, $\mathbf{\Sigma}_{\text{iso}} = \text{diag}([\frac{1}{3}, \frac{1}{3}, \frac{1}{3}])$, and $\mathbf{\Sigma}_{\text{aniso}} = \text{diag}([\frac{1}{11}, \frac{1}{11}, \frac{9}{11}])$ in the case of anisotropic positional noise. For each case of certain percentage of outliers and positional error type, $N_{trail} = 100$ registration trials have been conducted. For each registration trial, (i) the target registration error (TRE) values are computed, where we consider all the model points $\mathbf{Y}$ is the interested targets $\text{TRE} = ||\mathbf{R}_{\text{est}}\mathbf{r}_i + \mathbf{t}_{\text{est}} - \mathbf{R}_{\text{true}}\mathbf{r}_i - \mathbf{t}_{\text{true}}||$, where $\mathbf{r}_i \in \mathbb{R}^3$ is the interested target in the model frame (i.e., $\mathbf{Y}$); (ii) the rotational and translation error values are computed as follows: $\text{err}_{\text{rot}} = \frac{\arccos[\frac{\text{trace}(\mathbf{R}_{\text{true}}\mathbf{R}_{\text{est}}^{\text{T}})-1}{2}]}{\pi} \times 180^\circ$, where $\mathbf{R}_{\text{true}} \in SO(3)$ and $\mathbf{R}_{\text{est}} \in SO(3)$ denote the ground-truth and estimated rotation matrices respectively and $\text{err}_{\text{trans}} = ||\mathbf{t}_{\text{true}} - \mathbf{t}_{\text{est}}||_2$, where $\mathbf{t}_{\text{true}}$ and $\mathbf{t}_{\text{est}}$ denote the ground-truth and estimated translation vectors, respectively. The mean values associated with the N_{trial} registration trials are computed and recorded. We compare several state-of-the-art (SOTA) registration methods: ICP [25], CPD [12], ECMPR [39], Go-ICP [26], JRMPC [28], DGR [31], HMM(Iso) [40]. Among them, (1) HMM(Iso) is the SOTA registration one that also utilizes normal vectors [40];

(2) DGR [31] is the state-of-the-art learning-based method.

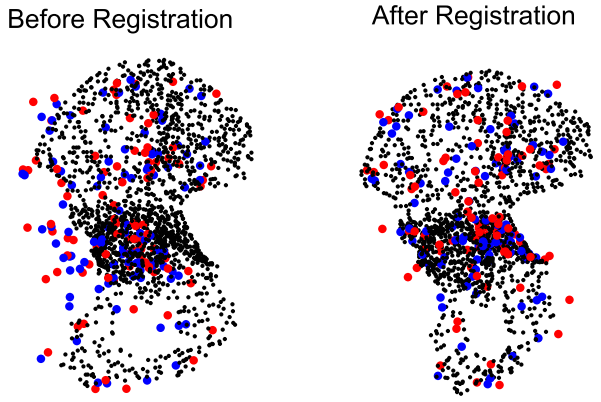

Fig. 2. The qualitative performances of the proposed method on the human pelvis model point sets (PSs), where 90% outliers exist in the intra-operative PSs $\mathbf{X}$. The pre-operative PS $\mathbf{Y}$, inlier and outlier intra-operative PSs $\mathbf{X}$ are denoted with black, blue and red dots respectively. (Left) The two PSs before registration. (Right) The two PSs after registration. As can be seen, the intra-operative inlier points (blue) are well matched with their corresponding black points after registration.

A. Pelvis Point Set (Full to Full Registration)

Quantitative Results: Table I shows both the rotational and translational error values on the human pelvis PS.As it can be seen from Table I, the proposed approach (1) achieves the lowest values in terms of both rotational and translational error in nearly all test cases; (2) is robust to increasing percentages of outliers while others are not. Table II (upper) includes the corresponding TRE values under various cases of noise and outliers. It can

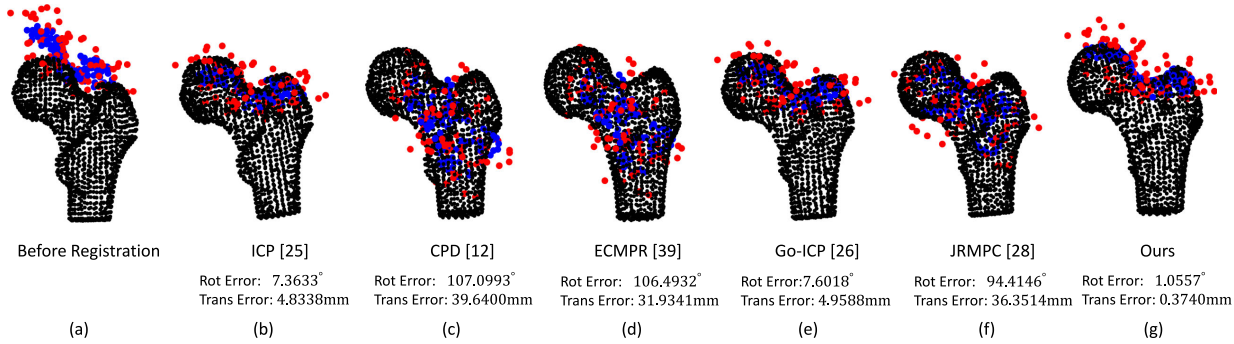

Fig. 3. The registration qualitative performances on the human femur model point sets (PSs). (a) The pre-operative and intra-operative PSs before registration. The two PSs after registration using (b) ICP, (c) CPD, (d) ECMPR, (e) Go-ICP, (f) JRMPC, (g) our methods. In all sub-figures, the black points represent the pre-operative model PS, the blue shows the intra-operative inlier points while the red shows the intra-operative outliers. The rotational error in degree and translational error values in milimeters are shown for all compared methods. As can be seen from the sub-figures, our proposed approach can well align the partial intra-operative inlier PS (denoted as blue points) with the pre-operative model (denoted as black points) while the other methods fail.

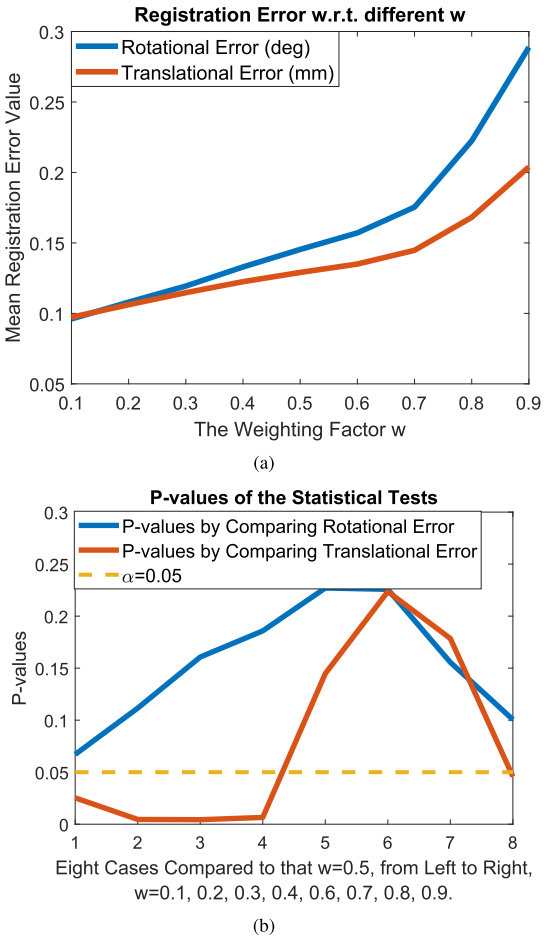

Fig. 4. In this figure, 30% outliers exist in $\mathbf{D}_x$ on the human pelvis model. (a) The blue and red lines show that the mean rotational and translation error values with respect to different values of w. Both the rotational and translation error values increase slightly when w is increased from 0.1 to 0.9. (b) The p-values of tests by comparing results at $w = 0.5$ and those eight cases with those at $w = 0.1, 0.2, 0.3, 0.4, 0.6, 0.7, 0.8, 0.9$, respectively. The blue line indicates that there is no significant differences between different cases of w in terms of the translation error. The red line indicates that cases where $w = 0.1, 0.2, 0.3, 0.4$ are significantly different from that where $w = 0.5$ while cases where $w = 0.6, 0.7, 0.8, 0.9$ are different from that where $w = 0.5$ in terms of the rotational error.

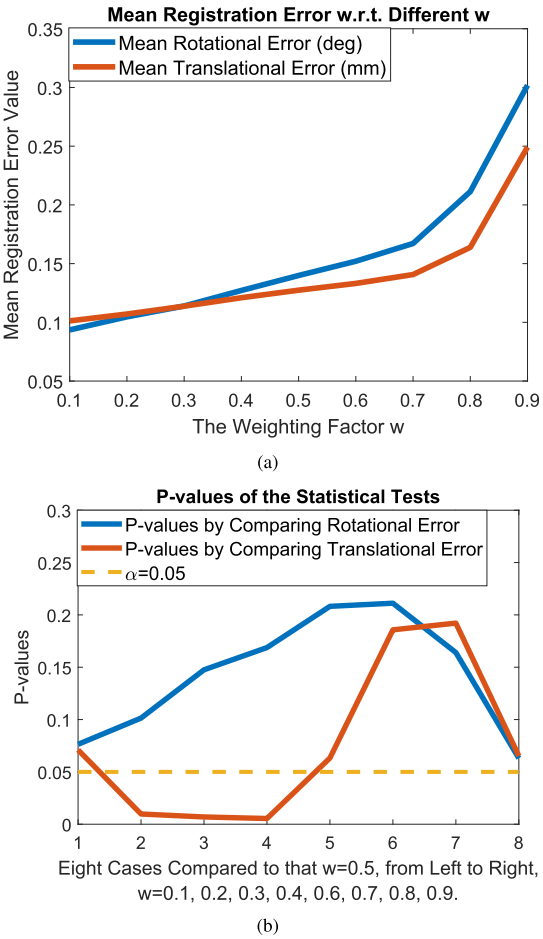

Fig. 5. In this figure, 50% outliers exist in $\mathbf{D}_x$ on the human pelvis model. (a) The blue and red lines show that the mean rotational and translation error values with respect to different values of w. Both the rotational and translation error values increase slightly when w is increased from 0.1 to 0.9. (b) The p-values of tests by comparing results at $w = 0.5$ and those at $w = 0.1, 0.2, 0.3, 0.4, 0.6, 0.7, 0.8, 0.9$, respectively. The blue line indicates that there is no significant differences between different cases of w in terms of the translation error. The red line indicates that cases where $w = 0.2, 0.3, 0.4$ are significantly different from that where $w = 0.5$ while cases where $w = 0.1, 0.6, 0.7, 0.8, 0.9$ are not significantly different from that where $w = 0.5$ in terms of the rotational error.

be seen from Table II, the maximum TRE value is 0.7559 mm among all test cases, which satisfies the requirement of CAS [6], [10]. **Qualitative Results:** Fig. 2 shows the qualitative results with our proposed approach. As it can be seen from Fig. 2 (right), the two PSs were accurately registered even with very large percentage of outliers in the data PS (90 outlier points exist in $\mathbf{X}$).

B. Femur Point Set (Partial to Full Registration)

Quantitative Results: In this experiment, the intra-operative human femur PS covers a partial region of the full pre-operative model PS. The mean rotational error value of the five cases of percentages of outliers (i.e., 10%, 30%, 50%, 70%, 90%) is 0.3768° and 0.4086° while the mean translational error value is 0.2336 mm and 0.4393 mm, for isotropic and anisotropic positional noise respectively. Table II (below) includes the corresponding TRE values, where the maximum TRE value is 0.8275 mm. **Qualitative Results:** Fig. 3 show the qualitative results on the femur PS. As it can be seen from Fig. 3, the two PSs were successfully registered even with large percentage of outliers in the data PS (i.e., 90% outliers or 90 outlier points in $\mathbf{X}$) with our proposed approach while other methods fail.

C. Robustness to w

The proposed approach's robustness to the weight of outliers w in the HMM $p(\mathbf{d}_n^x|\mathbf{D}_y, \mathbf{\Theta})$ in Equation (2) is also tested. The rotational and translational error values at $w = 0.5$ are compared with those at $w = 0.1, 0.2, 0.3, 0.4$ and at $w = 0.6, 0.7, 0.8, 0.9$, and paired-t tests are conducted to see if their differences are significant. Fig. 4 (a) includes the rotational and translational error values at different w on the pelvis model with 30% outliers and isotropic noise in $\mathbf{D}_x$. Fig. 4 (b) includes the corresponding p-values, with eight values for either rotational (blue) or translation (red) error. Fig. 5 (a) includes the rotational and translational error values at different w on the pelvis model with 50% outliers and isotropic noise in $\mathbf{D}_x$. Fig. 5 (b) includes the corresponding p-values of the paired t-tests. As can be seen from Fig. 4 and Fig. 5, both the rotational and translational error values increase with larger w. To emphasize, two further observations can be made from Fig. 4 and Fig. 5, (1) the differences between the rotational error values associated with different w are not statistically different with those at $w = 0.5$; (2) the translational error values associated with more than 50% cases are not statistically different with those at $w = 0.5$. To conclude, the values of w will not influence the registration accuracy significantly.

VI. Conclusions

This paper introduces a novel normal-assisted rigid registration approach where the anisotropic positional uncertainty is considered and normal vectors are undirected. Results on the human pelvis and femur bone models demonstrate the proposed approach's significant improved performances over the existing methods and potential applications in computer-assisted surgery (CAS).

Appendix

A. Derivation of p_{mn} in (5)

The posteriors p_{mn} is computed based on the Bayes' rule.

$$p_{mn} = \frac{\frac{w}{M} g e^{-\frac{1}{2}\mathbf{z}_{mn}^{\mathsf{T}}\mathbf{\Sigma}^{-1}\mathbf{z}_{mn}} e^{\kappa\left((\mathbf{R}\widehat{\mathbf{y}}_m)^{\mathsf{T}}\widehat{\mathbf{x}}_n\right)^2}}{\sum_{m=1}^{M} \frac{w}{M} g e^{-\frac{1}{2}\mathbf{z}_{mn}^{\mathsf{T}}\mathbf{\Sigma}^{-1}\mathbf{z}_{mn}} e^{\kappa((\mathbf{R}\widehat{\mathbf{y}}_m)^{\mathsf{T}}\widehat{\mathbf{x}}_n)^2} + (1-w)\frac{1}{N}} = \frac{g e^{-\frac{1}{2}\mathbf{z}_{mn}^{\mathsf{T}}\mathbf{\Sigma}^{-1}\mathbf{z}_{mn}} e^{\kappa\left((\mathbf{R}\widehat{\mathbf{y}}_m)^{\mathsf{T}}\widehat{\mathbf{x}}_n\right)^2}}{\sum_{m=1}^{M} g e^{-\frac{1}{2}\mathbf{z}_{mn}^{\mathsf{T}}\mathbf{\Sigma}^{-1}\mathbf{z}_{mn}} e^{\kappa((\mathbf{R}\widehat{\mathbf{y}}_m)^{\mathsf{T}}\widehat{\mathbf{x}}_n)^2} + \frac{(1-w)M}{wN}}, \tag{14}$$

where $g = \frac{1}{(2\pi)^{\frac{3}{2}}|\mathbf{\Sigma}|^{\frac{1}{2}}} W(\frac{1}{2}, \frac{3}{2}, \kappa)^{-1}$, $\mathbf{z}_{mn} = \mathbf{x}_n - \mathbf{R}\mathbf{y}_m - \mathbf{t}$.

B. Derivation of $Q(\mathbf{\Theta})$ in (3)

Following the standard EM procedure, the objective function $Q(\mathbf{\Theta})$ in (3) is formulated by constructing the complete negative likelihood. By assuming that all data points are independent, $p(\mathbf{D}_x|\mathbf{D}_y, \mathbf{\Theta}) = \prod_{n=1}^{N} p(\mathbf{d}_n^x|\mathbf{D}_y, \mathbf{\Theta})$. Then we take the "ln" operation on both sides, $\ln p(\mathbf{D}_x|\mathbf{D}_y, \mathbf{\Theta}) = \sum_{n=1}^{N} \ln p(\mathbf{d}_n^x|\mathbf{D}_y, \mathbf{\Theta}) = \sum_{n=1}^{N}((1-w)\sum_{m=1}^{M} p(\mathbf{d}_n^x|z_n = m, \mathbf{\Theta}) + w\frac{1}{N})$. For clarity, we provide the detailed expression of $\ln p(\mathbf{d}_n^x|z_n = m, \mathbf{\Theta})$ as $-\frac{1}{2}\ln|\mathbf{\Sigma}| - \frac{1}{2}\mathbf{z}_{mn}^{\mathsf{T}}\mathbf{\Sigma}^{-1}\mathbf{z}_{mn} - \ln W(\frac{1}{2}, \frac{3}{2}, \kappa) + \kappa((\mathbf{R}\widehat{\mathbf{y}}_m)^{\mathsf{T}}\widehat{\mathbf{x}}_n)^2$. The expected negative log likelihood $Q(\mathbf{\Theta})$ to be minimized is the following $\sum_{n,m=1}^{N,M} p_{mn}(\frac{1}{2}\ln|\mathbf{\Sigma}| + \frac{1}{2}\mathbf{z}_{mn}^{\mathsf{T}}\mathbf{\Sigma}^{-1}\mathbf{z}_{mn} + \ln W(\frac{1}{2}, \frac{3}{2}, \kappa) - \kappa((\mathbf{R}\widehat{\mathbf{y}}_m)^{\mathsf{T}}\widehat{\mathbf{x}}_n)^2)$.

C. Matrix Forms of r_1 and r_2

Let us construct the matrix $\mathbf{B} \in \mathbb{R}^{M\times N}$ as follows,

$$\mathbf{B} = \begin{bmatrix} (\mathbf{R}\widehat{\mathbf{y}}_1)^{\mathsf{T}}\widehat{\mathbf{x}}_1 & \dots & (\mathbf{R}\widehat{\mathbf{y}}_1)^{\mathsf{T}}\widehat{\mathbf{x}}_N \\ . & \dots & . \\ . & \dots & . \\ . & \dots & . \\ (\mathbf{R}\widehat{\mathbf{y}}_M)^{\mathsf{T}}\widehat{\mathbf{x}}_1 & \dots & (\mathbf{R}\widehat{\mathbf{y}}_M)^{\mathsf{T}}\widehat{\mathbf{x}}_N \end{bmatrix} \in \mathbb{R}^{M\times N}, \tag{15}$$

whose matrix form $\mathbf{B} = (\mathbf{R}\widehat{\mathbf{Y}})^{\mathsf{T}}\widehat{\mathbf{X}}$. With $\mathbf{B}$, we can get the matrix form of r_1 in Section. IV-D as $r_1 = (\mathbf{e}^{\mathsf{T}}\mathbf{B} \circ \mathbf{B} \circ \mathbf{P})/N_{\mathbf{P}}$. On the other hand, r_2 is computed as, $r_2 = \frac{\text{trace}(\mathbf{P}\mathbf{X}_{\text{ave}}^{\mathsf{T}}\mathbf{R}\mathbf{Y}_{\text{ave}})}{\mathbf{norm}_y^{\mathsf{T}}\mathbf{Y}\mathbf{norm}_x^{\mathsf{T}}}$, where $\mathbf{X}_{\text{ave}} \in \mathbb{R}^{3\times N}$ and $\mathbf{Y}_{\text{ave}} \in \mathbb{R}^{3\times M}$ denote the de-meaned positional and normal vectors, $\mathbf{X}_{\text{ave}} = \mathbf{X} - \boldsymbol{\mu}_x\mathbf{1}_N^{\mathsf{T}}$, $\mathbf{Y}_{\text{ave}} = \mathbf{Y} - \boldsymbol{\mu}_y\mathbf{1}_M^{\mathsf{T}}$, where $\mathbf{1}_N \in \mathbb{R}^{N\times 1}$ and $\mathbf{1}_M \in \mathbb{R}^{M\times 1}$ are vectors with all elements being 1, and the weighted mean vectors $\boldsymbol{\mu}_x \in \mathbb{R}^3$ and $\boldsymbol{\mu}_y \in \mathbb{R}^3$ of $\mathbf{X}$ and $\mathbf{Y}\boldsymbol{\mu}_x = \mathbf{X}\mathbf{1}_N/N$, $\boldsymbol{\mu}_y = \mathbf{Y}\mathbf{1}_M/M$, and $\mathbf{norm}_x \in \mathbb{R}^{N\times 1}$ and $\mathbf{norm}_y \in \mathbb{R}^{M\times 1}$ store the norms of the positional vectors in $\mathbf{X}$ and $\mathbf{Y}$.

References

[1] á. P. Bustos and T.-J. Chin, "Guaranteed outlier removal for point cloud registration with correspondences," *IEEE Trans. Pattern Anal. Mach. Intell.*, vol. 40, no. 12, pp. 2868–2882, Dec. 2018.

[2] R. H. Taylor, A. Menciassi, G. Fichtinger, P. Fiorini, and P. Dario, "Medical robotics and computer-integrated surgery," in *Handbook of Robotics*, Springer, 2016, pp. 1657–1684.

[3] M. Berger *et al.*, "A survey of surface reconstruction from point clouds," *Comput. Graph. Forum*, vol. 36, no. 1, pp. 301–329, 2017.

[4] L. Han, L. Xu, D. Bobkov, E. Steinbach, and L. Fang, "Real-time global registration for globally consistent RGB-D slam," *IEEE Trans. Robot.*, vol. 35, no. 2, pp. 498–508, Apr. 2019.

[5] M. R. Robu *et al.*, "Global rigid registration of CT to video in laparoscopic liver surgery," *Int. J. Comput. Assist. Radiol. Surg.*, vol. 13, no. 6, pp. 947–956, 2018.

[6] F. J. Lawin, M. Danelljan, F. S. Khan, P.-E. Forssen, and M. Felsberg, "Density adaptive point set registration," in *Proc. IEEE Conf. Comput. Vis. Pattern Recognit.*, 2018, pp. 3829–3837.

[7] J.-X. Zhao, C. Li, H. Ren, M. Hao, L.-C. Zhang, and P.-F. Tang, "Evolution and current applications of robot-assisted fracture reduction: A comprehensive review," *Ann. Biomed. Eng.*, vol. 48, no. 1, pp. 203–224, 2020.

[8] Z. Min, H. Ren, and M. Q. Meng, "Statistical model of total target registration error in image-guided surgery," *IEEE Trans. Automat. Sci. Eng.*, vol. 17, no. 1, pp. 151–165, Jan. 2020.

[9] J. Luo *et al.*, "Using the variogram for vector outlier screening: Application to feature-based image registration," *Int. J. Comput. Assist. Radiol. Surg.*, vol. 13, no. 12, pp. 1871–1880, 2018.

[10] Z. Min, J. Wang, and M. Q.-H. Meng, "Robust generalized point cloud registration using hybrid mixture model," in *Proc. IEEE Int. Conf. Robot. Automat.*, 2018, pp. 4812–4818.

[11] H. Ren and P. Kazanzides, "Investigation of attitude tracking using an integrated inertial and magnetic navigation system for hand-held surgical instruments," *IEEE/ASME Trans. Mechatronics*, vol. 17, no. 2, pp. 210–217, Apr. 2012.

[12] A. Myronenko and X. Song, "Point set registration: Coherent point drift," *IEEE Trans. Pattern Anal. Mach. Intell.*, vol. 32, no. 12, pp. 2262–2275, Dec. 2010.

[13] G. K. Tam *et al.*, "Registration of 3D point clouds and meshes: A survey from rigid to nonrigid," *IEEE Trans. Vis. Comput. Graph.*, vol. 19, no. 7, pp. 1199–1217, Jul. 2013.

[14] J. Ma, W. Qiu, J. Zhao, Y. Ma, A. L. Yuille, and Z. Tu, "Robust L2E estimation of transformation for non-rigid registration," *IEEE Trans. Signal Process.*, vol. 63, no. 5, pp. 1115–1129, Mar. 2015.

[15] J. Ma, J. Wu, J. Zhao, J. Jiang, H. Zhou, and Q. Z. Sheng, "Nonrigid point set registration with robust transformation learning under manifold regularization," *IEEE Trans. Neural Netw. Learn. Syst.*, vol. 30, no. 12, pp. 3584–3597, Dec. 2019.

[16] J. Ma, X. Jiang, J. Jiang, J. Zhao, and X. Guo, "LMR: Learning a two-class classifier for mismatch removal," *IEEE Trans. Image Process.*, vol. 28, no. 8, pp. 4045–4059, Aug. 2019.

[17] J. Ma, J. Zhao, J. Jiang, H. Zhou, and X. Guo, "Locality preserving matching," *Int. J. Comput. Vis.*, vol. 127, no. 5, pp. 512–531, 2019.

[18] I. Machado *et al.*, "Deformable MRI-ultrasound registration using correlation-based attribute matching for brain shift correction: Accuracy and generality in multi-site data," *NeuroImage*, vol. 202, 2019, Art no. 116094.

[19] L. Zhou, S. Wang, and M. Kaess, "A fast and accurate solution for pose estimation from 3D correspondences," in *Proc. IEEE Int. Conf. Robot. Automat.*, 2020, pp. 1308–1314.

[20] J. Wu, M. Liu, Z. Zhou, and R. Li, "Fast symbolic 3D registration solution," *IEEE Trans. Automat. Sci. Eng.*, vol. 17, no. 2, pp. 761–770, Apr. 2020.

[21] J. Wu, "Rigid 3D registration: A simple method free of SVD and eigen-decomposition," *IEEE Trans. Instrum. Meas.*, vol. 69, no. 10, pp. 8288–8303, Apr. 2020.

[22] K. Mardia and I. Dryden, "The complex watson distribution and shape analysis," *J. Roy. Stat. Soc., Ser. B Stat. Methodol.*, vol. 61, no. 4, pp. 913–926, 1999.

[23] Z. Min and M. Q.-H. Meng, "Robust generalized point set registration using inhomogeneous hybrid mixture models via expectation maximization," in *Proc. Int. Conf. Robot. Automat.*, 2019, pp. 8733–8739.

[24] H. Yang, J. Shi, and L. Carlone, "TEASER: Fast and certifiable point cloud registration," *IEEE Trans. Robot.*, vol. 37, no. 2, pp. 314–333, Apr. 2021.

[25] Z. Zhang, "Iterative point matching for registration of free-form curves and surfaces," *Int. J. Comput. Vis.*, vol. 13, no. 2, pp. 119–152, 1994.

[26] J. Yang, H. Li, D. Campbell, and Y. Jia, "Go-ICP: A globally optimal solution to 3D ICP point-set registration," *IEEE Trans. Pattern Anal. Mach. Intell.*, vol. 38, no. 11, pp. 2241–2254, Nov. 2016.

[27] O. Hirose, "A Bayesian formulation of coherent point drift," *IEEE Trans. Pattern Anal. Mach. Intell.*, vol. 43, no. 7, pp. 2269–2286, Jul. 2021.

[28] G. D. Evangelidis and R. Horaud, "Joint alignment of multiple point sets with batch and incremental expectation-maximization," *IEEE Trans. Pattern Anal. Mach. Intell.*, vol. 40, no. 6, pp. 1397–1410, Jun. 2018.

[29] Y. Wang and J. M. Solomon, "Deep closest point: Learning representations for point cloud registration," in *Proc. IEEE Int. Conf. Comput. Vis.*, 2019, pp. 3523–3532.

[30] Y. Wang and J. M. Solomon, " PRNet: Self-supervised learning for partial-to-partial registration," in *Proc. Adv. Neural Inf. Process. Syst.*, 2019, pp. 8814–8826.

[31] C. Choy, W. Dong, and V. Koltun, "Deep global registration," in *Proc. IEEE/CVF Conf. Comput. Vis. Pattern Recognit.*, 2020, pp. 2514–2523.

[32] J. Ma, X. Jiang, A. Fan, J. Jiang, and J. Yan, "Image matching from handcrafted to deep features: A survey," *Int. J. Comput. Vis.*, vol. 129, no. 1, pp. 1–57, 2020.

[33] S. Billings and R. Taylor, "Generalized iterative most likely oriented-point (G-IMLOP) registration," *Int. J. Comput. Assist. Radiol. Surg.*, vol. 10, no. 8, pp. 1213–1226, 2015.

[34] Z. Min, J. Wang, S. Song, and M. Q.-H. Meng, "Robust generalized point cloud registration with expectation maximization considering anisotropic positional uncertainties," in *Proc. IEEE/RSJ Int. Conf. Intell. Robots Syst.*, 2018, pp. 1290–1297.

[35] N. Ravikumar, A. Gooya, A. F. Frangi, and Z. A. Taylor, "Generalised coherent point drift for group-wise registration of multi-dimensional point sets," in *Proc. Int. Conf. Med. Image Comput. Comput.-Assist. Intervent.*, Springer, 2017, pp. 309–316.

[36] N. Ravikumar, A. Gooya, S. Çimen, A. F. Frangi, and Z. A. Taylor, "Group-wise similarity registration of point sets using student's t-mixture model for statistical shape models," *Med. Image Anal.*, vol. 44, pp. 156–176, 2018.

[37] Z. Min, J. Wang, and M. Q. Meng, "Joint rigid registration of multiple generalized point sets with hybrid mixture models," *IEEE Trans. Automat. Sci. Eng.*, vol. 17, no. 1, pp. 334–347, Jan. 2020.

[38] S. Sra and D. Karp, "The multivariate watson distribution: Maximum-likelihood estimation and other aspects," *J. Multivariate Anal.*, vol. 114, pp. 256–269, 2013.

[39] R. Horaud, F. Forbes, M. Yguel, G. Dewaele, and J. Zhang, "Rigid and articulated point registration with expectation conditional maximization," *IEEE Trans. Pattern Anal. Mach. Intell.*, vol. 33, no. 3, pp. 587–602, Mar. 2011.

[40] Z. Min, J. Wang, and M. Q. Meng, "Robust generalized point cloud registration with orientational data based on expectation maximization," *IEEE Trans. Automat. Sci. Eng.*, vol. 17, no. 1, pp. 207–221, Jan. 2020.